Macromolecules

ARTICLE

pubs.acs.org/Macromolecules

Structure of Polymer Tethered Highly Grafted Nanoparticles

Vivek Goel,[†] Joanna Pietrasik,[‡,§] Hongchen Dong,[§] Jitendra Sharma,[†] Krzysztof Matyjaszewski,[§] and Ramanan Krishnamoorti*[,†]

[†]Department of Chemical Engineering, University of Houston, Houston, Texas 77204, United States

[‡]Department of Chemistry, Institute of Polymer and Dye Technology, Technical University of Lodz, 90 924 Lodz, Poland

[§]Department of Chemistry, Carnegie Mellon University, Pittsburgh, Pennsylvania 15213, United States

ABSTRACT: Spherical nanoparticles of silica grafted with a dense brush of low-polydispersity polymers prepared by living radical polymerization are shown to form ordered crystalline structures. The minimum distance between nanoparticle surfaces, a good measure of the end-to-end distance of the tethered polymers, scales as the square root of the molecular weight of the polymer chains. The blending of the grafted nanoparticles with homopolymers of matched and mismatched molecular weights indicates that the crystalline order persists even with high amounts of homopolymer added and for such diluted systems with as little as 0.7 vol % silica.

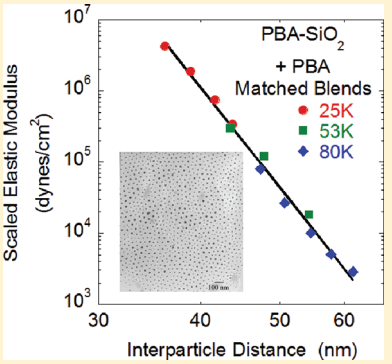

INTRODUCTION

A central issue in the development of reinforced and multifunctional organic−inorganic nanocomposites has been the ability to disperse and control the three-dimensional arrangement of the nanoparticles.[1,2] In particular, the crystallization of dilute quantities of nanoparticles with exquisite control of the interparticle distance is an important technical challenge.[3,4] Colloidal crystals have been formed at high concentrations and more recently at low concentrations with the aid of polymer grafted colloidal particles dispersed as concentrated, semidilute, or dilute solutions.[2,5,6] In such grafted colloidal particles, crystallization is thought to occur by a soft repulsive potential due to the grafted chains, unlike the case of usual colloidal crystals wherein crystallization is thought to occur either by short-range hard-sphere interactions or by long-range electrostatic interactions.[3,6]

In this paper we report a strategy to create crystals of spherical ∼15 nm diameter silica nanoparticles, with as little as 0.7 vol % of silica nanoparticles, stabilized with a high density of nearly monodisperse polymer chains grafted from the surface by the use of atom transfer radical polymerization methods.[7−9] Furthermore, these hybrid materials provide an ideal framework to examine the structural behavior of highly grafted polymers attached to a convex surface and challenge the theoretically predicted behavior of such systems.[10,11] Such hybrids, combining the behavior of linear polymer chains and hard-sphere character of nanoparticles, are capable of bridging much of our understanding of colloidal dispersions and that of star polymers.[12] Finally, we demonstrate a soft repulsive interaction potential between the grafted nanoparticles is indeed responsible for the observed crystallization behavior.

EXPERIMENTAL SECTION

Materials. *n*-Butyl acrylate (BA, Acros, 99%), styrene (S) (Aldrich, 99%), and acrylonitrile (AN) (Acros, 99%) were purified by filtration through a basic alumina column to remove inhibitors before the synthesis. The procedure for the synthesis of 1-(chlorodimethylsilyl)propyl 2-bromoisobutyrate and the subsequent functionalization of the silica (30 wt % silica in methyl isobutyl ketone, effective diameter D = 16.5 nm, MIBK-ST, Nissan) was derived from a previously described method.[9] Bis(2-pyridylmethyl)octadecylamine (BPMODA), tris(2-pyridylmethyl)amine (TPMA), and tris(2-(dimethylamino)ethyl)amine (Me_6TREN) were synthesized according to the literature.[13] CuBr (Aldrich, 99%) was purified via several slurries in acetic acid followed by filtration and washing with methanol and ethyl ether and was stored under nitrogen before use. $CuBr_2$ (Aldrich, 99.999%), $CuCl_2$ (Acros, 99%), polyoxyethylene (20) oleyl ether (Brij 98, Aldrich), hexadecane (Aldrich), L-ascorbic acid (AA, Aldrich, 99%), dimethyl-2,6-dibromoheptanedioate (DMDBrHD, Aldrich, 97%), *N*,*N*,*N*′,*N*′,*N*″-pentamethyldiethylenetriamine (PMDETA, Aldrich, 99%), ethyl 2-bromoisobutyrate (EBiB) (Acros, 98%), 2,2′-bipyridine (bpy), 4,4′-dinonyl-2,2′-bipyridine (dNbpy) (Aldrich, 97%), tin(II) 2-ethylhexanoate ($Sn(EH)_2$) (Aldrich), anisole (Aldrich), and hydrofluoric acid (50 vol % HF, Acros) were used as received.

Synthesis. Poly(*n*-butyl acrylate) homopolymer brushes were synthesized by activators generated by electron transfer (AGET) ATRP of BA from 2-bromoisobutyrate functionalized silica particles in miniemulsion under conditions similar to those reported previously[14] or in solution. The detailed reaction conditions are listed in Table 1. When BA

Received: March 17, 2011
Revised: September 1, 2011
Published: September 16, 2011

Table 1. ATRP of BA and SAN from Functionalized Silica Particles or from Small Molecular Weight Initiator

entry[a]	media	initiation	[BA]:[S]:[AN]:[initiator]	$M_{n,SEC}$ (g/mol)	M_w/M_n	no. of tethered chains/particle
1	solution, 20% vol solvent	AGET	600:0:0:1	3 900[b]	1.20	~600
2	miniemulsion	AGET	200:0:0:1	24 700[b]	1.27	~600
3	miniemulsion	AGET	600:0:0:1	53 500[b]	1.25	~600
4	miniemulsion	AGET	600:0:0:1	79 400[b]	1.29	~600
5	solution, 10% vol solvent	normal	150:0:0:1	21 100	1.07	
6	solution, 50% vol solvent	normal	300:0:0:1	55 000	1.23	
7	solution, 50% vol solvent	normal	400:0:0:1	79 600	1.09	
8	solution, 50% vol solvent	normal	0:200:130:1	1 800[b]	1.08	~400
9	solution, 50% vol solvent	normal	0:200:130:1	22 000[b]	1.21	~400
10	solution, 50% vol solvent	ARGET	0:2000:1300:1	137 200[b]	1.34	~400

[a] Entry 1, AGET ATRP in solution; [SiO_2-Br]:[$CuCl_2$]:[TPMA]:[$Sn(EH)_2$] = 1:2:2:0.6, 60 °C, acetone/anisole. Entries 2−4, AGET ATRP in miniemulsion; [SiO_2-Br]:[$CuBr_2$]:[BPMODA]:[AA] = 1:0.5:0.5:0.2, 80 °C, hexadecane 5 wt % based on monomer, Brij 98−14 wt % solid content. Entries 5−7, normal ATRP; [SiO_2-Br]:[CuBr]:[PMDETA] = 1:1:1, 70 °C, anisole. Entry 8, normal ATRP; [SiO_2-Br]:[CuBr]:[bpy] = 1:3:6, 70 °C, anisole. Entry 9, normal ATRP; [SiO_2-Br]:[CuBr]:[dNbpy] = 1:4:8, 80 °C, anisole. Entry 10, ARGET ATRP; [SiO_2-Br]:[$CuCl_2$]:[Me_6TREN]:[$Sn(EH)_2$] = 1:0.1:1.0:1.0, 80 °C, anisole. [b] Polymers were analyzed after etching silica with HF.

hybrids were synthesized in solution, a Schlenk flask was charged with TPMA ligand (149.2 mg, 0.575 mmol), $CuCl_2$ catalyst (69.2 mg, 0.575 mmol), and silica macroinitiator (504.0 mg, 0.288 mmol of Br); then 3.5 mL of anisole and 2.0 mL of acetone were added, and the contents were stirred until a homogeneous solution formed. Next *n*-butyl acrylate (22.0 mL, 172.8 mmol) was added to the flask. The resulting mixture was degassed by four freeze−pump−thaw cycles. After melting the mixture, a solution of $Sn(EH)_2$ (55.94 μL, 0.173 mmol) in anisole (0.5 mL) was added. The sealed flask was placed in thermostated oil bath at 60 °C. Samples were taken at timed intervals to follow the progress of the reaction. The polymerization was stopped by opening the flask and exposing the catalyst to air. The hybrid material was purified by precipitation into cold methanol several times.

In the case of synthesis of PBA homopolymer, the polymerization was carried out at 70 °C. DMDBrHD (56.6 μL, 0.26 mmol), PMDETA (54.4 μL, 0.26 mmol), BA (11 mL, 78 mmol), and anisole (1.1 mL) were added to a 25 mL Schlenk flask equipped with a magnetic stir bar. The flask was sealed, and the resulting solution was subjected to three freeze−pump−thaw cycles. After equilibration at room temperature, CuBr (37.3 mg, 0.26 mmol) was added to the solution under nitrogen flow, and the flask was placed in preheated oil bath. Aliquots were removed by syringe in order to monitor molecular weight evolution. After a predetermined time, the flask was removed from the oil bath and opened to expose the catalyst to air. The polymerization solution was diluted with $CHCl_3$ and passed over an alumina (activated neutral) column to remove the catalyst. Solvent was removed by rotary evaporation, and the polymer was isolated by precipitation into cold methanol.

Poly(styrene-*co*-acrylonitrile) copolymer brushes were grafted from 2-bromoisobutyrate functionalized silica particles via normal and ARGET (activators regenerated by electron transfer) ATRP. The detailed reaction conditions are listed in Table 1. In a typical normal ATRP of styrene and acrylonitrile (Table 1, entry 8), a Schlenk flask was charged with bpy ligand (155.6 mg, 0.996 mmol) and silica macroinitiator (470.4 mg, 0.166 mmol Br), then anisole (5.50 mL) was added, and the contents were stirred until a homogeneous solution formed. Next, styrene (4.0 mL, 0.0349 mmol) and acrylonitrile (1.52 mL, 0.0231 mmol) were added to the flask. After three freeze−pump−thaw cycles, the flask was filled with nitrogen; then while the mixture was immersed in liquid nitrogen, 71.4 mg (0.498 mmol) of CuBr was added. The flask was sealed with a glass stopper, evacuated, and backfilled four times with nitrogen. After melting the reaction mixture and warming to the room temperature, the sealed flask was placed in thermostated oil bath at 70 °C. Samples were taken at timed intervals to follow the progress of the reaction. The polymerization was stopped by opening the flask and exposing the catalyst to air. The hybrid material was purified by precipitation into methanol with several times.

ARGET ATRP of S and AN was used for the synthesis of high-molecular-weight PSAN copolymer brushes from silica surfaces (Table 1, entry 10). Styrene (4.0 mL, 0.0349 mol), acrylonitrile (1.52 mL, 0.0231 mol), and anisole (4.52 mL) were added to a dry Schlenk flask. Then, the silica macroinitiator (50.3 mg, 0.0177 mmol Br) and a solution of $CuCl_2$ (0.238 mg, 1.77 μmol)/Me_6TREN (0.47 μL, 1.77 μmol) complex in anisole (0.8 mL) were added. The resulting mixture was degassed by four freeze−pump−thaw cycles. After melting the mixture, a solution of $Sn(EH)_2$ (5.73 μL, 0.0177 mmol) and Me_6TREN (4.20 μL, 0.0159 mmol) in anisole (0.2 mL) was added. The sealed flask was placed in thermostated oil bath at 80 °C. Samples were taken at timed intervals to follow the progress of the reaction. The polymerization was stopped by opening the flask and exposing the catalyst to air. The hybrid material was purified by precipitation into methanol several times.

Characterization. Molecular weight (M_n) and molecular weight distribution (M_w/M_n) were determined by GPC equipped with an autosampler (Waters, 717 plus), HPLC pump with THF as eluent at 1 mL/min (Waters, 515), and four columns (guard, 10^5 Å, 10^3 Å, 100 Å; Polymer Standards Services) in series. Toluene was used as internal standard. Calculations of molar mass were determined using PSS software using a calibration based on linear polystyrene standards. Polymers were analyzed after etching silica with HF. On the basis of elemental analysis there was 4.1 and 2.8 wt % Br, i.e., 0.5106 mmol Br/1 g silica or 0.3530 mmol Br/1 g silica, corresponding to ~1500 and ~1000 initiating sites per silica particle, providing ~600 and ~400 tethered chains per silica particles after polymerization, respectively.

RESULTS AND DISCUSSION

The structure of the polymer tethered silica hybrid nanoparticles is characterized using small-angle X-ray and neutron scattering (SAXS and SANS, respectively) and corroborated using transmission electron microscopy (TEM). The SAXS data for a series of poly(*n*-butyl acrylate) (PBA)-based silica hybrids (grafting density $\sigma \sim 0.8$ chain/nm^2; $d_0 \sim 16.5$ nm; 600 chains per nanoparticle) (Figure 1a) indicates the presence of an ordered structure with the clear presence of both first- and second-order intensity peaks, whose *q*-values, as noted in Table 2, decrease with increasing chain length of the attached polymer. The SAXS data for these melt-state PBA-based hybrids are

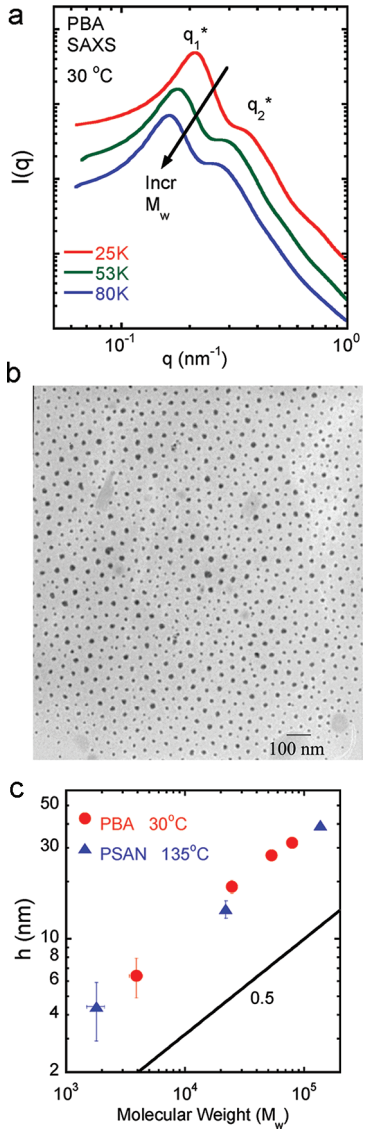

Figure 1. (a) Small-angle X-ray scattering data for three PBA−SiO_2 hybrids with varying molecular weight of the grafted PBA chains. The nanoparticles employed and the surface density of initiators on the silica particle are identical in each case. The intensity data were shifted for clarity. (b) TEM of an unstained 80K-based PBA−SiO_2 hybrid thin film (sectioned by cryo-microtoming) that is consistent with the SAXS data and demonstrates a well-ordered structure. (c) The minimum distance between the spherical nanoparticles, h (obtained from eq 1), is a good measure of the brush height and is shown for the PBA−SiO_2 and PSAN−SiO_2 hybrids (with 16.5 nm diameter SiO_2 nanoparticles and containing ∼1000 chains/nanoparticle) as a function of molecular weight of the nearly monodisperse polymer chain attached to the silica nanoparticles.

virtually independent of temperature between 20 and 180 °C and reflect the well-equilibrated nature of the structure and the possible thermodynamic origins for the development of the structure. We note that repeated annealing in the presence of solvent vapors and at high temperatures did not yield any change in the nature of the small-angle peak or the electron microscopy images. While these data indicate that $q_1^*:q_2^* :: 1:\sqrt{3}$ for all the hybrids examined, extremely weak higher order scattering peaks at $\sim\sqrt{7}q_1^*$ are discernible and suggest an ordered liquid lattice

Table 2. Structural Characterization of Silica−Poly(*n*-butyl acrylate) Nanocomposites

sample	mol wt M_n	$\phi_{SiO_2} \times 100$	q_1^*	q_2^*	q_2^*/q_1^*	$S(q_1^*)$
PBA4K	3 900	33	0.334	0.571	1.71	5.4 ± 0.2
PBA25K	24 700	8.5	0.212	0.363	1.71	9.9 ± 0.3
PBA53K	53 500	3.9	0.177	0.305	1.72	9.3 ± 0.2
PBA80K	79 400	2.7	0.163	0.281	1.72	8.4 ± 0.2

with weak FCC or random close packed ordering.[15] The A15 lattice can be eliminated based on the absence of a $(5/2)^{1/2}$ reflection, and BCC can be eliminated due to the absence of the $\sqrt{2}$ reflection. Similar FCC crystalline order has been reported by Ohno et al. for 300−850 nm diameter SiO_2 particles grafted with PMMA and dispersed in a good solvent.[6]

We further employ the empirical Hansen−Verlet criterion, which states that the value of the structure factor $S(q)$ at q_1^* is ∼2.85 at the melting transition,[16] to test if indeed these hybrids crystallize or form liquidlike order. From the SAXS and SANS data, the values of $S(q=q_1^*)$ were calculated (Table 2) by dividing the measured intensity by the form factor corresponding to individual spherical particles obtained from dilute solution scattering measurements, and they indicate that as per the Hansen−Verlet criterion the PBA based hybrids are crystalline. We further note that linear viscoelastic stress−relaxation measurements previously published on these samples,[17] with a dynamic time range of 0.1−100 000 s (significantly longer than the polymer relaxation time which range from milliseconds to 0.1 s for the molecular weights examined here), indicate the presence of an elastic solid for all of these samples, consistent with the notion of the crystalline arrangement of the silica nanoparticles.

TEM (Figure 1b) of bulk samples (sections created by cryo-microtoming) and from thin films deposited from solution indicate agreement with the scattering measurements and the Hansen−Verlet criterion.[16] The presence of a hexagonal arrangement of the silica nanoparticles with significant polycrystallinity is clearly observed. Such ordering has been previously observed in several other material systems: in colloidal and nanoparticle dispersions at high volume fractions of the nanoparticles, in block copolymer solutions and melts with microphase separation, and in high-arm content star polymer systems among other soft matter systems.[2,6,18] Similar to the block copolymer systems, in the absence of attractive interactions between the nanoparticles, the origins of the crystalline ordering for the hybrid nanoparticles result from entropic repulsion, connectivity, and volume filling constraints.[19] Nevertheless, the unique features in the hybrids described here are (a) the low volume fraction of the silica nanoparticles (as low as 0.027 corresponding to the pure hybrid with 80K chains attached and extendable down to 0.007 corresponding to the PBA80K hybrid diluted by 75% by free 80K chains as shown below) where we observe ordering and (b) the core and corona size scales are comparable and the core and corona are sharply separated with no interpenetration of the core by the corona chains.

From the scattering data, we estimate the minimum distance between silica nanoparticles, h, as

$$h = a\left(\frac{2\pi}{q_1^*}\right) - d_0 \qquad (1)$$

where a is 1.22 for an FCC lattice or 1.23 for structures dominated by two-body correlations, and d_0 corresponds to the diameter of

the silica nanoparticles, in this case estimated on the basis of scattering and microscopy data to be 16.5 ± 1.5 nm.[15] Considering that the hybrids here consist of polymer melts with *no* dispersing low molecular weight solvent or dispersant, the value of h is a good measure of the size of the polymer chains tethered to the silica but is not equivalent to the radius of gyration of the polymer or the brush height. The molecular weight dependence of the scaling of h is shown in Figure 1c for the PBA series of hybrids and for a comparable series of poly(styrene-*co*-acrylonitrile) (PSAN) hybrids. For these PSAN hybrids the measurements reported here are in the melt state of the polymer (T = 150 °C). The extent of ordering as observed by the value of the peak intensity of the primary correlation peak and the presence and intensity of the second-order reflections for the PSAN-based system are significantly poorer, possibly due to the lower graft density and the high glass transition temperature in the PSAN case, than those reported for the PBA hybrids. Nevertheless, the values of h scales as $\sim M_n^{\alpha}$, with α = 0.50 ± 0.04 for the PBA series and 0.51 ± 0.06 for the PSAN series over roughly 1 decade in molecular weight, with the values for h for the PSAN series being somewhat lower than that of the PBA series for comparable molecular weights. We note, however, that in spite of the observed scaling behavior of the distance between particles with molecular weight is similar to unperturbed chains in the melt, the chains are indeed stretched: For example, for the 80K sample, the value of h is ∼30 nm while a calculation of the unperturbed R_g indicates a value of ∼8 nm and, even assuming no interpenetration, a chain stretching of ∼2, at the least.

The "blob model" of Daoud and Cotton for star polymers and curved brushes in their melt state provides a reasonable theoretical framework to consider the results presented here, although the thickness of the studied brushes (h = 4−30 nm) is comparable to the core diameter d_0 = 16.5 nm.[10,20] The Daoud and Cotton model suggests that for the case of dense melts of stars with significant overlap between branch chains the brush height scales as approximately $f^{1/2} + N^{1/2}$, where f is the number of branches and N is a measure of the degree of polymerization. Thus, for a star polymer melt with significant branch overlap and with constant number of branches, we predict that the radius of the star polymer scales with molecular weight of arm molecular weight as $\sim M_n^{1/2}$ and that the chains are indeed stretched as compared to homopolymers of comparable molecular weight. While previous experimental studies for ∼125 arm star polymer (polybutadiene) *melts* indicated a rough scaling exponent of 0.35 for the size of the stars with molecular weight,[15] our current results for the case of polymer brushes on a silica nanoparticle with a particle diameter comparable to the brush height yields a scaling of $N^{1/2}$. We note that in the case studied here the measurements allow for a direct measure of the distance beween particles and not directly the size of the polymer chains. Further, the extended nature of the polymer chains near the particle and the directionality of the polymer necessitated by the pinning of one end of the polymer at the nanoparticle must distort the conformational statistics of the polymer. Nevertheless, while the scaling observed is temptingly similar to that expected for melt brushes with significant interpenetration, we caution that such a scaling might purely fortuitous as the number of branches is quite large and the range of molecular weights studied and their comparable length with the particle size would suggest that we are not truly in the limit of melt stars. It is entirely possible that the systems studied are in the crossover regime between flat brushes (i.e., brush height ≪ particle size) and those of true stars (i.e., brush height ≫ particle size). One final note in the comparison between the results presented here and those of the PB stars reported previously,[15] the PB stars do not exhibit a second-order scattering peak, except for the lowest molecular weight sample, and examination of the scattering intensity suggests a failure to meet the criteria of Hansen and Verlet to classify those materials as crystalline ordered materials.

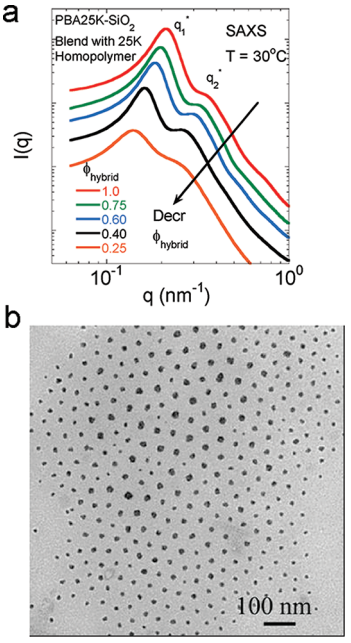

Figure 2. (a) SAXS data for a series of matched blends of a homopolymer of PBA (25K) with the PBA25K−SiO_2 hybrid. With increasing homopolymer content, the interparticle distance increases (swelling of the lattice) with the crystalline order persisting to high homopolymer addition. The intensity data were shifted vertically to improve clarity. (b) TEM of a 40% PBA80K−SiO_2 hybrid blended with 60% PBA (80K) homopolymer indicating the presence of a well-defined crystal structure for such blends.

An alternate mechanism to control the distance between the hybrid nanoparticles was achieved by blending the hybrids with the untethered (free) polymers of similar (matched) or higher (mismatched) molecular weight. Such a study as outlined below not only allows us to test ideas of homopolymer miscibility with a brush but also enables the elucidation of the melting of the crystalline structure adopted by the hybrid nanoparticles. For the matched blend systems, as observed in Figure 2, with increasing amount of added homopolymer the value of q_1^* decreases, implying a swelling of the interparticle distance, and a second-order peak at $\sim\sqrt{3}q_1^*$ is observed for all blends. We note that at even at the highest quantities of added homopolymer the intensity at small angle is well-behaved and does not show any divergence, suggesting that at all compositions the blends remain homogeneous. We examine two issues concerning such matched blends in Figure 3.

First, the values of $S(q_1^*)$ for these matched blends, like those for the pure hybrids, are large and decrease with increasing homopolymer content. Applying the Hansen−Verlet criterion for the melting transition, the data in Figure 3a suggests that for volume fractions of hybrid material $\phi_{hybrid}(=(1-\phi_{homopolymer}))$ > 0.25, the blends are crystalline, and only for cases where they are diluted with more than 75 vol % homopolymer do they

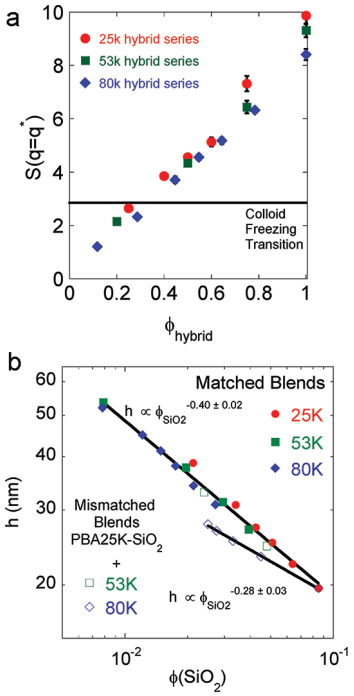

Figure 3. (a) Examination of $S(q=q_1^*)$ for the different matched blends in the context of the Hansen−Verlet criterion for crystallization. (b) Examination of the minimum interparticle separation distance (h), a measure of the brush height and interpenetration of the brushes by the free homopolymer chains for the matched (closed symbols) and mismatched blends (open symbols), with varying homopolymer dilution.

undergo melting. The full width at half-maximum (fwhm) of the primary scattering peak increases slightly with increasing homopolymer content and undergoes a significant change for mixtures with more than ∼75 vol % homopolymer, consistent with the application of the Hansen−Verlet criterion described above. This crystalline order, even at relatively high homopolymer content, is further supported by electron micrographs shown in Figure 2b. Interestingly, the melting composition does not show strong molecular weight dependence.

Second, the variation of the minimum distance between two silica particles, h, that is a direct measure of the brush height (Figure 3b) with matched molecular weight dilution is examined. While h increases with increasing homopolymer content in each case (approximately described by $\phi_{\text{hybrid}}^{\sim -(0.44 \pm 0.05)}$), plotting the data with respect to the bare silica content (i.e., the inorganic core volume fraction) allows for a simple superpositioning of all the values of h onto a single master plot. Considering that the initiator grafted silica nanoparticles used in each of these experiments come from the same batch, and the virtually identical polymerization conditions employed,[8] the appropriate invariant to employ is indeed the silica amount (volume or weight fraction). For the matched blends, the scaling with silica volume fraction, suggested by Figure 3b, is

$$h \propto \phi_{SiO_2}^{-(0.40 \pm 0.02)} \tag{2}$$

Such a scaling relationship suggests that the addition of matched molecular weight free chains to the highly grafted curved brushes leads to a swelling of the interparticle distance. If the free chains of matched molecular weight incorporated into the brush behaved as ideal chains, we would expect the brush height to

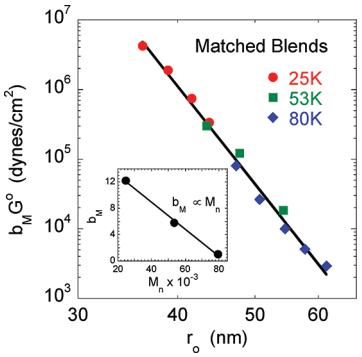

Figure 4. Dependence of the time-independent linear modulus for the hybrids and the matched blends as a function of the center-to-center distance of the lattice responsible for the elastic response. The moduli values for the three different series were shifted using a vertical shift factor to collapse the data on to the PBA80K matched series, and these shift factors are shown in the inset of the figure.

scale with molecular weight with a −1/3 exponent. This would suggest that the hybrid nanoparticles are acting as good solvents for the homopolymer chains and result in an expansion of the matched molecular weight chains.

On the other hand, we have also examined the case where the free chains are larger than the grafted chains. Specifically, we blend the 53K and 80K homopolymers to the PBA25K-based hybrid material and examine the structures formed. While the addition of the 53K homopolymer leads to a brush height scaling that is similar to that of the matched systems, the mixtures of 80K homopolymer and the PBA25K-based hybrid lead to a somewhat lower brush height and a scaling that is given as

$$h_{80K/PBA25K-hybrid} \propto \phi_{SiO_2}^{-(0.28 \pm 0.03)} \tag{3}$$

and indicating that the 80K homopolymer is akin to a poor solvent for the PBA25K-based silica hybrid. Such dewetting behavior of highly grafted brushes with high molecular weight homopolymers is quite similar to the behavior of spherical block copolymers, where a molecular weight discrepancy of a factor of 5 is tolerated prior to demixing.[21]

We return to the observation of the crystalline ordering observed in these hybrid materials for silica volume fractions down to 0.007 (PBA80K hybrid diluted with 75% 80K PBA homopolymer). As noted previously and demonstrated in a previous publication,[17] these hybrid materials exhibit an elastic response in linear viscoelastic measurements whose time scales far exceeds the longest relaxation time of the polymer chains. The time-independent elastic moduli (G°) observed from linear stress−relaxation measurements are an excellent tool to probe the interparticle interactions in such hybrids and their blends via[22]

$$G^\circ = \frac{1}{r_0}\left[\frac{\partial^2 U(r)}{\partial r^2}\right]_{r=r_0} \tag{4}$$

While the values of G° for the three series of matched blends, described in a previous publication,[17] when plotted against r_0 demonstrate parallel power-law behavior, we empirically separate the molecular weight effect and silica contribution and collapse the curves by a modulus shift factor, b_M, that is only a function of the molecular weight of the grafted chains. We plot the values of the rescaled $b_M G^\circ$ as a function of the interparticle spacing (r_0) in

Figure 4 for all of the hybrids and matched blends studied here. We note in passing that the modulus scaling with grafted chain molecular weight is linear and surprisingly much weaker than those observed for sphere forming block copolymers or star polymers.[23] The interparticle distance dependence of the rescaled modulus is adequately represented by a power-law as $b_M G^\circ \propto r_0^{-(14.5\pm2.0)}$ and suggesting that the repulsive potential between the grafted nanoparticles scales as $U(r) \propto r^{-(12.5\pm2.0)}$. This interaction potential lies between those of the two limiting cases of common crystal formers in colloids and resembles only somewhat the exponential potential function used often to understand the behavior of star polymers. The effect of the finite impenetrable core and the high density of grafting probably contribute to this functional form of the potential, and understanding how this interaction potential changes systematically with grafting density and diameter of the core−inorganic nanoparticle and its consequences on the structural behavior of the hybrids and the behavior of the polymer chains in response will allow us to carefully tailor the ordering behavior of such grafted nanoparticles.

CONCLUDING REMARKS

We have examined the structure and dynamics of spherical nanoparticles of silica grafted with a dense brush of low-polydispersity polymers prepared by living radical polymerization and have shown that these form ordered crystalline ordered structures. The brush thickness, measured using the lattice distance between nanoparticles, scales as the square root of the molecular weight of the polymer chains. However, comparison to the unperturbed chain dimensions of untethered polymers indicates that the tethered chains are indeed stretched. The structural studies of the blends of the grafted nanoparticles with the corresponding matched and mismatched molecular weight homopolymers indicates that the crystalline order persists even with high amounts of homopolymer added and for systems with as little as 0.7 vol % silica. In a previous paper we have shown that the grafted nanoparticles with varying molecular weight of attached chains (with terminal relaxation times of <1 s, if not attached to the nanoparticle) and the blends with matched molecular weight homopolymers and high concentrations of the grafted nanoparticles demonstrate solidlike behavior for as long as 100 000 s.[17] Interpreting the modulus behavior as a function of nanoparticle lattice distance indicates that the potential between such grafted nanoparticles effectively scales as $U(r) \propto r^{-(12.5\pm2.0)}$. This suggests that such grafted nanoparticles are similar to common crystal formers in colloids and resemble only somewhat the exponential potential function used often to understand the behavior of star polymers. The effect of the finite impenetrable core and the high density of grafting probably contribute to this functional form of the potential, and understanding how this interaction potential changes systematically with grafting density and diameter of the core−inorganic nanoparticle and its consequences on the structural behavior of the hybrids and the behavior of the polymer chains in response will allow us to carefully tailor the ordering behavior of such grafted nanoparticles.

ACKNOWLEDGMENT

V.G., J.S., and R.K. gratefully acknowledge the support of the National Science Foundation (CMMI-0708096). J.P., H.D., and K.M. thank the Foundation for Polish Science and Ministry of Science and Higher Education and the National Science Foundation (DMR-05-49353) for their financial support. This work utilized neutron scattering facilities supported in by the NSF under Agreement DMR-0454672 and the X-ray beamline X27C at NSLS in the Brookhaven National Laboratory.

REFERENCES

(1) Krishnamoorti, R. *MRS Bull.* **2007**, *32* (4), 341–347. Jayaraman, A.; Schweizer, K. S. *Langmuir* **2008**, *24* (19), 11119–11130. Jayaraman, A.; Schweizer, K. S. *Macromolecules* **2008**, *41* (23), 9430–9438. Jayaraman, A.; Schweizer, K. S. *Mol. Simul.* **2009**, *35* (10−11), 835–848. Jayaraman, A.; Schweizer, K. S. *Macromolecules* **2009**, *42* (21), 8423–8434. Kumar, S. K.; Krishnamoorti, R. *Annu. Rev. Chem. Biomol. Eng.* **2010**, *1*, 37–58. Vaia, R. A.; Maguire, J. F. *Chem. Mater.* **2007**, *19* (11), 2736–2751.

(2) Yethiraj, A. *Soft Matter* **2007**, *3* (9), 1099–1115.

(3) Dach, B. I.; Rengifo, H. R.; Turro, N. J.; Koberstein, J. T. *Macromolecules* **2010**, *43* (16), 6549–6552. Wu, C. K.; Hultman, K. L.; O'Brien, S.; Koberstein, J. T. *J. Am. Chem. Soc.* **2008**, *130* (11), 3516–3520.

(4) Choi, J.; Dong, H.; Matyjaszewski, K.; Bockstaller, M. R. *J. Am. Chem. Soc.* **2010**, *132* (36), 12537–12539.

(5) Pusey, P. N.; Vanmegen, W. *Nature* **1986**, *320* (6060), 340–342. Yethiraj, A.; van Blaaderen, A. *Nature* **2003**, *421* (6922), 513–517. Ohno, K.; Morinaga, T.; Koh, K.; Tsujii, Y.; Fukuda, T. *Macromolecules* **2005**, *38* (6), 2137–2142. Ohno, K.; Morinaga, T.; Takeno, S.; Tsujii, Y.; Fukuda, T. *Macromolecules* **2006**, *39* (3), 1245–1249. Bourlinos, A. B.; Herrera, R.; Chalkias, N.; Jiang, D. D.; Zhang, Q.; Archer, L. A.; Giannelis, E. P. *Adv. Mater.* **2005**, *17* (2), 234–+.

(6) Ohno, K.; Morinaga, T.; Takeno, S.; Tsujii, Y.; Fukuda, T. *Macromolecules* **2007**, *40* (25), 9143–9150.

(7) Savin, D. A.; Pyun, J.; Patterson, G. D.; Kowalewski, T.; Matyjaszewski, K. *J. Polym. Sci., Part B: Polym. Phys.* **2002**, *40*, 2667–2676. Xia, J.; Matyjaszewski, K. *Macromolecules* **1999**, *32* (8), 2434–2437.

(8) Pyun, J.; Matyjaszewski, K. *Macromolecules* **2000**, *33*, 4039–4047.

(9) Pyun, J.; Jia, S.; Kowalewski, T.; Patterson, G. D.; Matyjaszewski, K. *Macromolecules* **2003**, *36* (14), 5094–5104.

(10) Forster, S.; Wenz, E.; Lindner, P. *Phys. Rev. Lett.* **1996**, *77* (1), 95–98.

(11) Biver, C.; Hariharan, R.; Mays, J.; Russel, W. B. *Macromolecules* **1997**, *30* (6), 1787–1792. Raphael, E.; Pincus, P.; Fredrickson, G. H. *Macromolecules* **1993**, *26* (8), 1996–2006.

(12) Likos, C. N.; Lowen, H.; Poppe, A.; Willner, L.; Roovers, J.; Cubitt, B.; Richter, D. *Phys. Rev. E* **1998**, *58* (5), 6299–6307. Likos, C. N.; Lowen, H.; Watzlawek, M.; Abbas, B.; Jucknischke, O.; Allgaier, J.; Richter, D. *Phys. Rev. Lett.* **1998**, *80* (20), 4450–4453. Shih, W. Y.; Shih, W. H.; Aksay, I. A. *Macromolecules* **1990**, *23* (13), 3291–3296. Vlassopoulos, D. *J. Polym. Sci., Part B: Polym. Phys.* **2004**, *42*, 2931–2941.

(13) Xia, J.; Matyjaszewski, K. *Macromolecules* **1999**, *32* (8), 2434–2437. Tyeklar, Z.; Jacobson, R. R.; Wei, N.; Murthy, N. N.; Zubieta, J.; Karlin, K. D. *J. Am. Chem. Soc.* **1993**, *115* (7), 2677–89. Pintauer, T.; Matyjaszewski, K. *Coord. Chem. Rev.* **2005**, *249* (11−12), 1155–1184.

(14) Bombalski, L.; Min, K.; Dong, H.; Tang, C.; Matyjaszewski, K. *Macromolecules* **2007**, *40* (21), 7429–7432.

(15) Vlassopoulos, D.; Kapnistos, M.; Fytas, G.; Roovers, J. *Macromol. Symp.* **2000**, *158*, 149–153.

(16) Hansen, J. P.; Verlet, L. *Phys. Rev.* **1969**, *184* (1), 151.

(17) Goel, V.; Pietrasik, J.; Matyjaszewski, K.; Krishnamoorti, R. *Ind. Eng. Chem. Res.* **2010**, *49* (23), 11985–11990.

(18) Lowen, H.; Watzlawek, M.; Likos, C. N.; Schmidt, M.; Jusufi, A.; Denton, A. R. *J. Phys.: Condens. Matter* **2000**, *12*, A465–A469. McConnell, G.; Lin, E. K.; Gast, A.; Huang, J. S.; Lin, M. Y.; Smith, S. D. *Faraday Discuss.* **1994**, *98*, 121–138. Sebastian, J. M.; Graessley, W. W.; Register, R. A. *J. Rheol.* **2002**, *46* (4), 863–879. Vega, D. A.; Sebastian, J. M.; Loo, Y.-L.; Register, R. A. *J. Polym. Sci., Part B: Polym. Phys.* **2001**, *39*, 2183–2197.

(19) Leibler, L. *Macromolecules* **1980**, *13*, 1602.

(20) Daoud, M.; Cotton, J. P. *J. Phys. (Paris)* **1982**, *43*, 531–538.

(21) Harton, S. E.; Kumar, S. K. *J. Polym. Sci., Part B: Polym. Phys.* **2008**, *46*, 351–358. Choi, S.; Lee, K. M.; Han, C. D.; Sota, N.; Hashimoto, T. *Macromolecules* **2003**, *36* (3), 793–803. Bodycomb, J.; Yamaguchi, D.; Hashimoto, T. *Macromolecules* **2000**, *33* (14), 5187–5197.

(22) Sebastian, J. M.; Lai, C.; Graessley, W. W.; Register, R. A. *Macromolecules* **2002**, *35*, 2707–2713.Callister, W. D. *Materials Science and Engineering: An Introduction*, 5th ed.; John Wiley & Sons Inc.: New York, 2000.

(23) Kossuth, M. B.; Morse, D. C.; Bates, F. S. *J. Rheol.* **1999**, *43* (1), 167–196.Mark, J. E.; Ngai, K. L.; Graessley, W. W.; Mandelkern, L.; Samulski, E.; Koenig, J.; Wignall, G. *Physical Properties of Polymers*, 3rd ed.; Cambridge University Press: Cambridge, UK, 2004.